DTU Library

Modeling of Ni Diffusion Induced Austenite Formation in Ferritic Stainless Steel Interconnects

Chen, Ming; Molin, Sebastian; Zhang, L.; Ta, Na; Hendriksen, Peter Vang; Kiebach, Wolff-Ragnar; Du, Y.

Modeling of Ni Diffusion Induced Austenite Formation in Ferritic Stainless Steel Interconnects

M. Chen[a], S. Molin[a], L. Zhang[b], N. Ta[a,b], P. V. Hendriksen[a], W. R. Kiebach[a], and Y. Du[b]

[a] Department of Energy Conversion and Storage, Technical University of Denmark
Roskilde 4000, Denmark
[b] State Key Laboratory of Powder Metallurgy, Innovative Materials Design Group
Central South University, Changsha, Hunan 410083, China

Ferritic stainless steel interconnect plates are widely used in planar solid oxide fuel cell (SOFC) or electrolysis cell (SOEC) stacks. During stack production and operation, nickel from the Ni/YSZ fuel electrode or from the Ni contact component diffuses into the IC plate, causing transformation of the ferritic phase into an austenitic phase in the interface region. This is accompanied with changes in volume and in mechanical and corrosion properties of the IC plates. In this work, kinetic modeling of the inter-diffusion between Ni and FeCr based ferritic stainless steel was conducted, using the CALPHAD approach with the DICTRA software. The kinetics of inter-diffusion and austenite formation was explored in full detail, as functions of layer thickness, temperature, time, and steel composition. The simulation was further validated by comparing with experimental results. Growth of the austenite phase in commercial interconnect materials is predicted to take place under practical stack operation conditions.

Introduction

Owing to high temperature stability and relatively low cost, chromia-forming ferritic stainless steels are widely used as interconnect materials in solid oxide fuel cell (SOFC) or electrolysis cell (SOEC) stacks. This type of steels has typically a chromium concentration of 20 - 30 wt.% and a close match of thermal expansion coefficient with the solid oxide cell (SOC) components (1). During high temperature oxidation, a chromia oxide scale is formed which offers a reasonably good electronic conductivity at SOFC/SOEC operating temperature (650-850°C) (2). For practical applications, protective coatings are required especially for the oxygen side, to further improve the oxidation resistance and the electrical conductivity of the formed oxide scale. Recent progress on alloy and coating development for ferritic stainless steel interconnects has been reviewed by Shaigan et al. (3).

In a so-called planar stack design, a certain number of planar SOCs are stacked together, with shaped interconnects in between. These interconnect plates serve as current collector and separator for the neighboring fuel and oxygen electrode compartments of two adjacent cells. An intimate contact between the cell component and the interconnect (IC) plate is therefore essential to ensure optimum cell and stack performance. During stack production and operation, inter-diffusion across the cell – IC interface takes place,

which under certain circumstances introduces adverse effects on the electrical, mechanical, and corrosion properties of the IC plates. One representative example is diffusion of nickel from the Ni/YSZ fuel electrode or from the Ni contact component into the IC plate, while iron and chromium from the steel diffuse in the reverse direction. Diffusion of Ni into the steel causes transformation of the ferritic BCC phase into the austenitic FCC phase in the interface region, accompanied with changes in volume and in mechanical and corrosion properties of the IC plates. A number of studies have been devoted to investigate this process experimentally. Sakai et al. reported a radial pattern of Ni diffusion into ZMG232 (4). Chromium depletion and internal oxidation occurred in the diffusion zone. Pre-oxidation of the steel was reported to be effective in suppressing the inter-diffusion, but resulted in an increase of the contact resistance. Quadakkers and his co-workers carried out detailed studies on characterizing Ni diffusion and formation of the austenite phase in long-term tested SOFC stacks and on model experiments of Ni mesh in contact with Crofer 22 APU or Crofer 22 H (2, 5). In addition to austenite, formation of sigma (σ) phase was detected in the interface region. The experiments were correlated to the thermodynamics of the Fe-Cr-Ni system. Authors of the current work have previously reported reduced oxidation kinetics in Ni electroplated Crofer 22 APU as compared to uncoated ones (6). This was attributed to slow diffusion kinetics of the FCC phase (2 - 3 magnitudes slower than in BCC). Recently, Harthøj et al. studied Ni diffusion from the Ni/YSZ fuel electrode into Crofer 22 APU and its influence on the contact resistance across the interface (7). It was concluded that the inter-diffusion introduces microstructural instability, but also lower electrical resistance (due to formation of metallic pathways). Similar studies have also been conducted by Mikkelsen et al. (8), who investigated long-term oxidation behavior and electrical interface resistance between FeCr alloy sheets and Ni/YSZ plates. Their results show that metallic bridges exist through the formed oxide scale even after 1 year of testing.

In this work, kinetic modeling of the inter-diffusion between Ni and FeCr based ferritic stainless steel was conducted, using the CALPHAD (CALculation of PHAse Diagrams) approach with the DICTRA software. To give a full account of the observed experimental phenomena, the following 3 processes have to be taken into account: inter-diffusion and transformation of ferrite into austenite, oxide scale formation, and formation of σ phase. The present work focuses on the first process only. Here kinetic modeling of inter-diffusion and austenite formation was explored in full detail, as functions of Ni contact component thickness, temperature, time, and steel composition. The simulation was further validated by comparing with experimental results. Growth of the austenite phase in commercial interconnect materials such as Crofer 22 APU is predicted under practical SOC operation conditions (i.e. in a temperature range of 700-900°C and a time frame of 1 hour – 5 years etc.). In the current work, the compositions are expressed in either mass fraction or mass percentage.

Experimental and Kinetic Modeling

We have previously reported oxidation kinetics of Ni coated Crofer 22 APU (ThyssenKrupp VDM, Germany) (6) in humidified H_2/N_2. The samples consisted of 300 μm thick Crofer 22 APU flat sheets electroplated with Ni on both sides. The oxidation study took place at 800°C in a mixture of 4 % H_2O + 9 % H_2 + 87 % N_2 for periods up to 2000 hours. In the present work, the post-mortem results obtained on the 13 μm thick Ni

coated Crofer 22 APU oxidized for 2000 h are employed to validate the modeling results. The polished cross-section was examined using a Supra 35 scanning electron microscope equipped with a field emission gun (FE-SEM, Carl Zeiss). Chemical compositions were obtained via an X-ray Energy Dispersive Spectrometer (EDS) with further data analysis using a microanalysis software NSS (Thermo Fischer Scientific Inc.).

The modeling part was carried out using the CALPHAD approach with the Thermo-Calc and DICTRA software (9). The thermodynamics and phase relations of relevant systems were explored using Thermo-Calc and TCFE7 database. For kinetic modeling, a 1D diffusion couple was set up (shown in Figure 1), where metallic Ni coating (austenite, FCC, denoted by γ in the current work) is in contact with FeCr-based ferritic stainless steel (ferrite, BCC, α). The inter-diffusion across the interface and the transformation of ferrite into austenite was modelled using DICTRA in conjunction with the MOBFE2 database. DICTRA is a software package for simulation of diffusional reactions in multicomponent alloys. For further detail on DICTRA, the readers are referred to the paper by Borgenstam et al. (10).
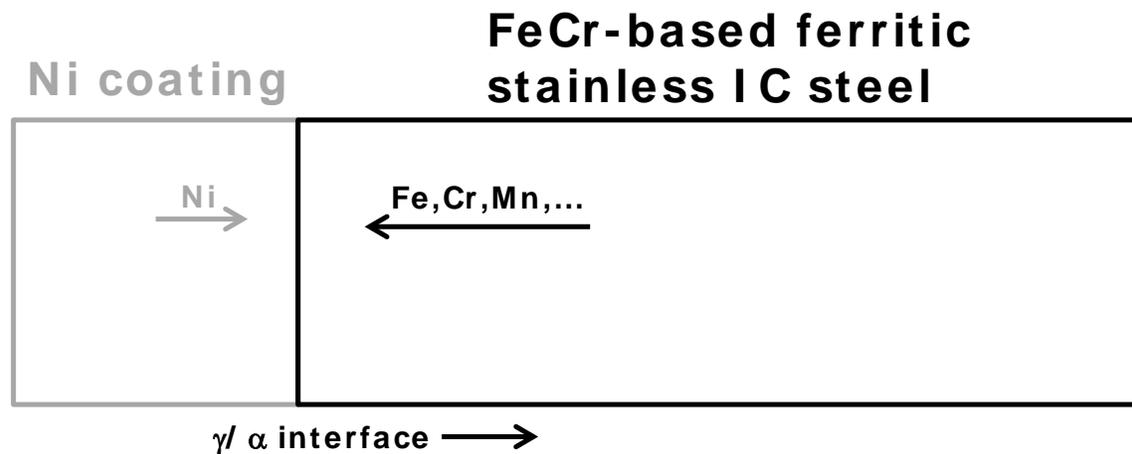

Figure 1. Schematic illustration of the diffusion couple between Ni coating (left) and FeCr-based ferritic stainless IC steel (right).

Results and Discussion

<u>Model Experiment of Ni Diffusion into Crofer 22 APU</u>

Figure 2 presents a SEM image on the polished cross-section of 13 μm Ni coated Crofer 22 APU after 2000 h oxidation at 800°C. The image was taken using back-scattered electron detector, where difference in contrast or greyness indicates different phases or compositions. As reported previously (6), the Ni coating remains metallic after electroplating. After 2000 h oxidation, most of Ni has diffused into the steel. A small number of Ni particles remains on the surface of the formed oxide scale. The oxide scale has a thickness of about 2 μm and has some tiny Ni particles as inclusions. Inside the steel, a contrast difference is found at a distance of 60-70 μm from the oxide scale – steel interface, indicating either phase and/or compositional change. The EDS elemental mapping of the scanned area is shown in Figure 3. The oxide scale consists of mainly Cr and Mn, corresponding to most likely an outer layer of $(Cr,Mn)_3O_4$ spinel and an inner

layer of Cr_2O_3, as reported previously (6). Inside the steel, the contrast difference observed in Figure 2 is reflected as change of Fe/Cr/Ni concentrations as shown in Figure 3. No secondary phase (e.g. σ phase) seems to appear in the examined area.

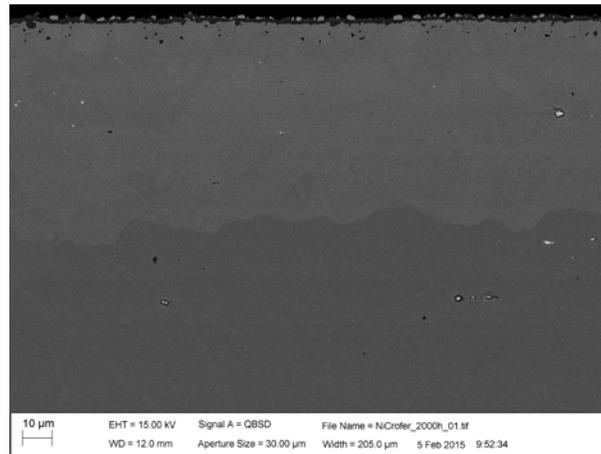Figure 2. SEM image on the polished cross-section of the oxide scale – steel (Crofer 22 APU) interface. The sample is a 300 μm thick Crofer 22 APU sheet coated with 13 μm thick Ni coating on both sides, further heat treated at 800^oC in $H_2+N_2+H_2O$ for 2000 h.
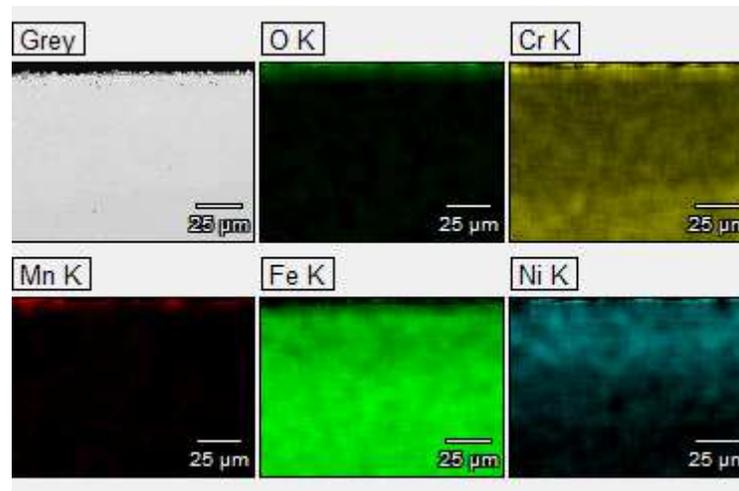

Figure 3. EDS elemental map on the cross-section of the oxide scale – steel (Crofer 22 APU) interface. The sample is a 300 μm thick Crofer 22 APU sheet coated with 13 μm thick Ni coating on both sides, further heat treated at 800^oC in $H_2+N_2+H_2O$ for 2000 h.

Based on the obtained area spectra imaging data, an integrated EDS line-scan was then made. The line was drawn perpendicular to the oxide scale – steel interface. The data over the entire area were then integrated along the line. Figure 4 plots the mass percentages of Fe, Cr, Ni, Mn from the oxide scale – steel interface into the steel, while the other elements are excluded. As expected, significant degree of inter-diffusion took place after 2000 h at 800^oC. The Ni content is still above 2 wt.% at a distance of ~100 μm from the oxide scale – steel interface, indicating Ni diffuses deeper. There seems to be a jump in the Ni content at the distance of 65 μm, in accordance with the contrast change shown in Figure 2.
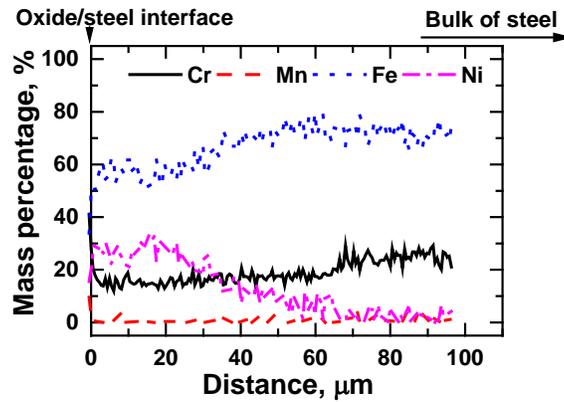
Figure 4. Integrated EDS line-scan perpendicular to the oxide scale – steel (Crofer 22 APU) interface. The sample is a 300 μm thick Crofer 22 APU sheet coated with 13 μm Ni coating on both sides, further heat treated at 800°C in $H_2+N_2+H_2O$ for 2000 h.

Phase Diagrams of Fe-Cr-Ni

The current work focuses on metallic phases of relevant systems. As shown in Figure 2, a thin layer of oxide scale formed on each side of the Ni coated steel sample. As compared to the 300 μm thick steel, the oxide scale has a thickness of only 4 μm (i.e. 2 μm on both sides) and is therefore expected to have a minor influence on the steel bulk composition. Formation of oxide scale may however have an influence on the local chemistry at the Ni – Steel interface. This will be considered in future work, when all the 3 processes (inter-diffusion and formation of austenite, oxidation, and formation of σ phase) will be modelled together. In the present work, the inter-diffusion and transformation of ferrite into austenite across the Ni – Steel interface is modelled. Figure 5 presents the phase diagram of Fe-Cr-Ni calculated at two different temperatures. At 800°C, the α phase has rather limited Ni solubility, while the γ phase, originating from pure Ni, has a wide solubility range for both Fe and Cr. The single-phase region of σ starts from the Fe-Cr binary and extends into the ternary, towards the Cr-rich corner. At 900°C, the σ single-phase region exists only in the ternary system. The 700°C phase diagram (not shown here) is similar to the one at 800°C, except that the solubility of Ni in the α phase is slightly higher.
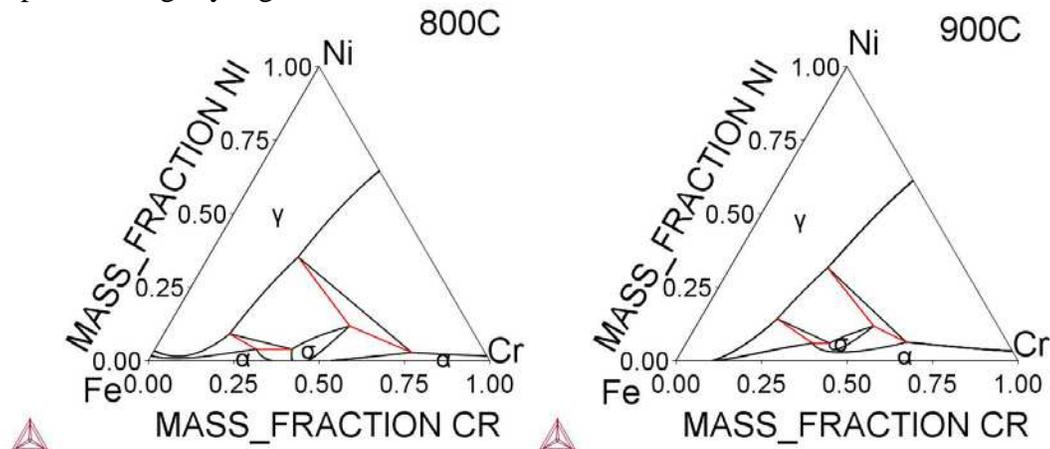

Figure 5. Phase diagrams of Fe-Cr-Ni at 800 and 900°C. In the diagrams all the single-phase regions have been marked: α - BCC (ferrite), γ - FCC (austenite), and σ. The red triangles indicate 3-phase equilibrium (α+γ+σ), while the remaining unmarked regions are 2-phase equilibria (α+γ, γ+σ, or α+σ).

Modeling of Ni Diffusion into $Fe_{0.77}Cr_{0.23}$ (Bulk Diffusion only)

As shown in Figure 1, in the current work, a diffusion couple of Ni – Steel was set up which mimics the experiments. As the experimental sample (Crofer 22 APU metal sheet, 300 μm in thickness) was coated with Ni on both sides, only half of the sample was modelled. Crofer 22 APU has about 20 – 24 wt.% Cr, 0.3 – 0.8 wt.% Mn plus some minor elements (La, Ti, etc.) and Fe as a balance (1, 2, 6). In the current work, first modeling was carried out on a diffusion couple of 13 μm Ni – 150 μm $Fe_{0.77}Cr_{0.23}$. Here only bulk diffusion is considered. The composition profiles along the diffusion couple at different time steps are presented in Figure 6 for periods up to 2000 h at 800°C. As expected, Ni diffuses into the steel while Fe and Cr diffuse in the reverse direction. In agreement with the thermodynamics (Figure 5), the content of Ni in the α phase (the right part of diffusion couple) is rather low all the way from the interface to the right boundary, while the contents of Fe and Cr in the γ phase decrease continuously.
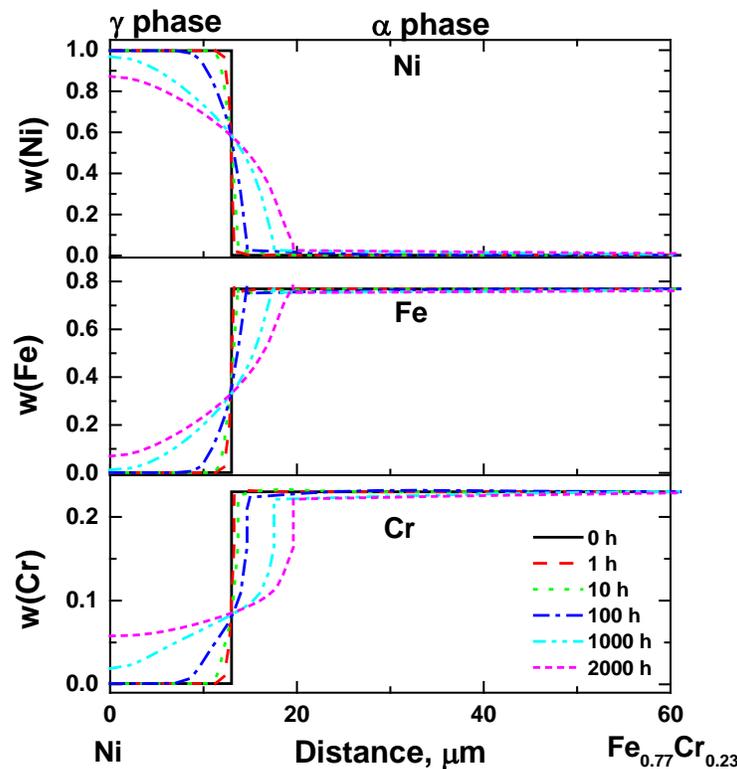

Figure 6. Calculated composition profiles (in mass fraction) along the diffusion couple of Ni – $Fe_{0.77}Cr_{0.23}$ heat treated at 800°C for periods up to 2000 h. The initial thickness was 13 μm and 150 μm for the Ni and $Fe_{0.77}Cr_{0.23}$ layers, respectively.

Based on the composition profiles, the Ni diffusion distance can then be evaluated as the distance from the original α/γ interface to the point where the Ni content in the γ phase reaches below 0.5 wt.%. The results are plotted in Figure 7a for 700, 800, and 900°C. At 800°C, a Ni diffusion distance of 71.6 μm is obtained from DICTRA modeling, where only bulk diffusion is considered. Accompanied with inter-diffusion, the α/γ interface moves towards the right. Figure 7b plots the thickness of the newly formed γ layer as a function of time at 700-900°C. After 2000 h at 800°C, a 6.6 μm thick α (steel)

layer is transformed into γ. According to the experimental results, the Ni diffusion distance in Crofer 22 APU is beyond 100 μm for 2000 h diffusion at 800°C. DICTRA modeling seems to under-estimate the inter-diffusion and hence also the accompanied α→γ phase transformation, when only bulk diffusion is considered.
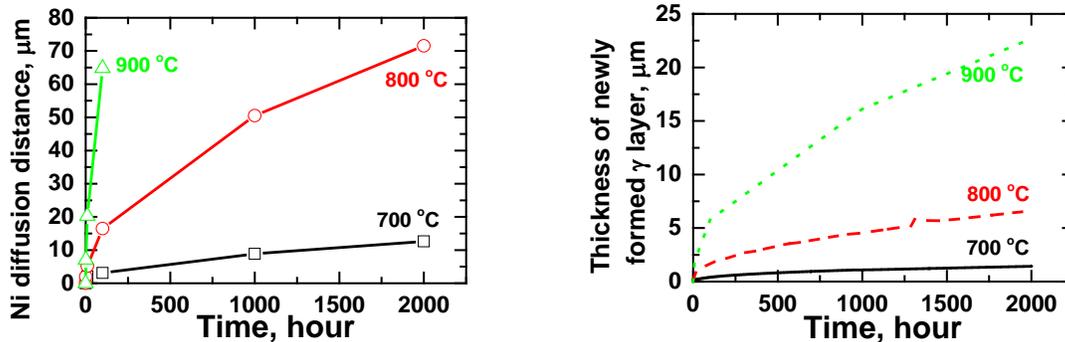

Figure 7. (a) Calculated Ni diffusion distance and (b) thickness of newly formed γ layer in the diffusion couple of Ni – $Fe_{0.77}Cr_{0.23}$ heat treated at 700-900°C for periods up to 2000 h. The initial thickness was 13 μm and 150 μm for the Ni and $Fe_{0.77}Cr_{0.23}$ layers, respectively. The Ni diffusion distance is defined as the distance between the initial γ/α interface (i.e. at 0 h) and the position where the Ni content reaches below 0.5 wt.%.
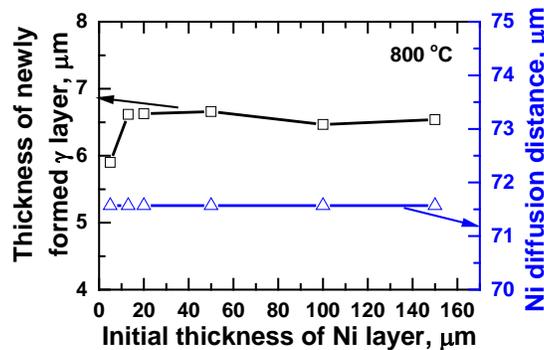

Figure 8. Calculated Ni diffusion distance and thickness of newly formed γ layer in the diffusion couple of Ni – $Fe_{0.77}Cr_{0.23}$ heat treated at 800°C for 2000 h. The initial thickness of the Ni layer was varied as 5, 13, 20, 50, 100, and 150 μm, while the initial thickness of the $Fe_{0.77}Cr_{0.23}$ layer was 150 μm.

In the current work, the influence of layer thickness is verified via DICTRA modeling. Here only the thickness of the Ni coating is varied from 5 to 150 μm. Its influence on Ni diffusion distance and the thickness of newly formed γ layer is shown in Figure 8, for a diffusion time of 2000 h at 800°C. The Ni diffusion distance is not influenced at all, as it is determined by the diffusion kinetics. The thickness of newly formed γ layer increases slightly when increasing the thickness of Ni coating from 5 to 13, but remains almost constant afterwards.

Modeling of Ni Diffusion into $Fe_{0.77}Cr_{0.23}$ (Bulk + Grain Boundary Diffusion)

To properly account the experimental data, grain boundary diffusion should be considered, which is an important and non-neglectable contribution especially at low temperature. The grain boundary diffusion model in DICTRA was then employed (10).

The grain boundary diffusion is correlated to the bulk diffusion by using the same frequency factor and modified bulk activation energy, as specified by the equation below:

$$M^{gb} = M_0^{bulk} \cdot \exp(F_{redGB} \cdot Q^{bulk}/R/T) \qquad [1]$$

where M^{gb} is the mobility in the grain boundary, M_0^{bulk} and Q^{bulk} is the frequency-factor and activation energy in the bulk respectively, and F_{redGB} is the bulk diffusion activation energy multiplier. The total mobility including both bulk and grain boundary diffusion is then formulated as:

$$M^{Total} = \delta/d \cdot M^{gb} + (1 - \delta/d) \cdot M^{bulk} \qquad [2]$$

where δ, d, and M^{bulk} are the grain boundary thickness, the grain size as a function of time and temperature, and the mobility in the bulk, respectively. The grain boundary diffusion model in DICTRA requires three input parameters: F_{redGB}, δ and d. In the current work, grain boundary diffusion is considered for both the α and γ phases. A grain size of 50 and 5 µm was adopted for the α and γ phase, respectively, according to the results reported by Garcia-Fresnillo et al. (2). The grain boundary thickness δ was set as $0.5 \cdot 10^{-10}$ m, as recommended by DICTRA. The bulk diffusion activation energy multiplier F_{redGB} was varied between 0.5 and 0.7. The best fit to the experimental data (shown in Figure 9a) was achieved at $F_{redGB} = 0.65$ for both α and γ phases. Figure 9a presents the calculated composition profile in comparison with the experimental results obtained from the present work (Figures 2-4). As shown in Figures 2-4, after 2000 h at 800°C, most of Ni has diffused into the steel and the original Ni – steel interface is replaced by the oxide scale – steel interface. This point was then set as "distance zero" as for the experimental data points. As shown in Figure 9, with the chosen parameters, the DICTRA modeling results are in reasonable agreement with the experimental ones. Distinct jumps are clearly shown in the concentration profile, which corresponds to the two end-points of the two phases in equilibrium (Figure 9b). The γ phase layer has grown to 63 µm in thickness (including the initial 13 µm Ni coating). By plotting the composition profile onto the ternary phase diagram, the diffusion path at different time steps can be illustrated. This is shown in Figure 9b. Four time steps are included: 1 h, 100 h, 2000 h, 5 years. At time = 0 h, the diffusion path starts from pure Ni and travels through the γ single-phase region all the way to the $\alpha+\gamma$ two-phase region and ends at the composition $Fe_{0.77}Cr_{0.23}$. The change to the diffusion path with time happens mainly in the γ single-phase region, which is due to its wide composition range and slower diffusion kinetics (two orders of magnitudes slower than that of the α phase). The diffusion path in the $\alpha+\gamma$ two-phase region moves slowly towards the $\alpha+\gamma+\sigma$ three-phase triangle. After 5 years, the diffusion path more or less coincides with the $\alpha+\gamma$ side of the $\alpha+\gamma+\sigma$ three-phase triangle. Thermodynamic calculations suggest that the equilibrium state of the given system (13 µm thick Ni + 150 µm thick $Fe_{0.77}Cr_{0.23}$) is a $\gamma+\sigma$ two-phase mixture. The diffusion process should then continue with formation of the σ phase and disappearance of the α phase. The diffusion path will travel through the $\alpha+\gamma+\sigma$ three-phase triangle and end in the $\gamma+\sigma$ two-phase region. To successfully model the entire process, diffusion in multi-phase mixtures should be properly accounted for. This will be presented in the future.
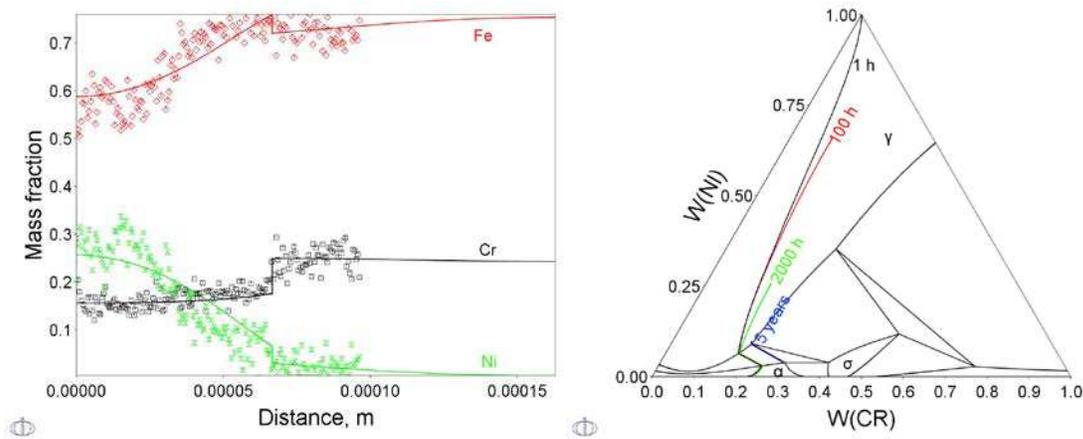
Figure 9. (a) Left: Calculated composition profiles (in mass fraction) along the diffusion couple of Ni – $Fe_{0.77}Cr_{0.23}$ heat treated at 800^oC for periods up to 2000 h. The initial thickness was 13 μm and 150 μm for the Ni and $Fe_{0.77}Cr_{0.23}$ layers, respectively. Both bulk and grain boundary diffusion are considered. The experimental data points are from the present work (Figure 4). Mn was excluded in calculating mass fraction; (b) Right: diffusion path at 1 h (black), 100 h (red), 2000 h (green), 5 years (blue) super-imposed onto the Fe-Cr-Ni phase diagram at 800^oC.

Modeling of Ni Diffusion into Crofer 22 APU ($Fe_{0.765}Cr_{0.23}Mn_{0.005}$)

Mn is also an important component of Crofer 22 APU, with a typical content of 0.3 – 0.8 wt.%. Its influence on inter-diffusion and austenite formation is further discussed in the following. A diffusion couple of 13 μm thick Ni – 150 μm thick $Fe_{0.765}Cr_{0.23}Mn_{0.005}$ (representing Crofer 22 APU) is set up and diffusion is allowed at 800^oC for 2000 h. The composition profile along the diffusion couple is plotted in Figure 10, along with that in Ni - $Fe_{0.77}Cr_{0.23}$. The two cases show very similar results, except that 0.5 wt.% Mn in the steel seems to promote the $\alpha \rightarrow \gamma$ transformation slightly, though the difference is rather small. Besides, Mn tends to enrich at the left boundary of the diffusion couple (i.e. in γ phase).
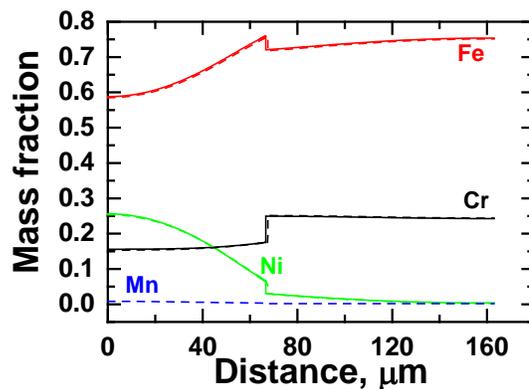

Figure 10. Calculated composition profiles (in mass fraction) along the diffusion couples of Ni – $Fe_{0.77}Cr_{0.23}$ (solid lines) and Ni – $Fe_{0.765}Cr_{0.23}Mn_{0.005}$ (dashed lines) heat treated at 800^oC for 2000 h. The initial thickness was 13 μm and 150 μm for the Ni and $Fe_{0.77}Cr_{0.23}$ or $Fe_{0.77}Cr_{0.23}Mn_{0.005}$ (Crofer 22 APU) layers, respectively. Both bulk and grain boundary diffusion are considered.

Conclusions

In the current work, the inter-diffusion between Ni and ferritic steel interconnects was investigated by both experiments and theoretical diffusion modeling employing DICTRA software and databases. The experimental results show that after 2000 h at 800°C Ni diffuses more than 100 μm deeper into Crofer 22 APU. DICTRA modeling gives a proper account of the experimental results on inter-diffusion and accompanied $\alpha \rightarrow \gamma$ phase transformation, when both bulk and grain boundary diffusion are considered. The inter-diffusion between Ni and Crofer 22 APU observed in the current work can be well explained by the thermodynamics and kinetics of the Fe-Cr-Ni system. The small amount of Mn in Crofer 22 APU seems to promote the $\alpha \rightarrow \gamma$ transformation slightly. DICTRA modeling further predicts enrichment of Mn towards Ni. The present work provides a proper account of the thermodynamics and kinetics of Ni-steel inter-diffusion and in addition provides input to further analysis of associated changes in the mechanical and corrosion properties of the IC plates.

Acknowledgments

References

1. M. Palcut, L. Mikkelsen, K. Neufeld, M. Chen, R. Knibbe, and P. V. Hendriksen, *Corros. Sci.*, **52**, 3309 (2010).
2. L. Garcia-Fresnillo, V. Shemet, A. Chyrkin, L. G. J. de Haart, and W. J. Quadakkers, *J. Power Sources*, **271**, 213 (2014).
3. N. Shaigan, W. Qu, D. G. Ivey, and W. Chen, *J. Power Sources*, **195**, 1529 (2010).
4. N. Sakai, T. Horita, K. Yamaji, Y. P. Xiong, H. Kishimoto, M. E. Brito, and H. Yokokawa, *Solid State Ionics*, **177**, 1933 (2006).
5. J. Froitzheim, L. Niewolak, M. Brandner, L. Singheiser, and W. J. Quadakkers, *J. Fuel Cell Sci. Technol.*, **7**, (2010).
6. S. Molin, M. Chen, J. R. Bowen, and P. V. Hendriksen, *ECS Trans.*, **57**, 2245 (2013).
7. A. Harthøj, H. Alimadadi, T. Holt, and P. Møller, *J. Electrochem. Soc.*, **162**, F387 (2015).
8. L. Mikkelsen, J. Hogh, and P. V. Hendriksen, in *8th European SOFC Forum*, p. A0905, Lucerne, Switzerland (2008).
9. J.-O. Andersson, T. Helander, L. Hoglund, P. Shi, and B. Sundman, *CALPHAD*, **26**, 273 (2002).
10. A. Borgenstam, L. Hoglund, J. Agren, and A. Engstrom, *J. Phase Equilib.*, **21**, 269 (2000).